Implementation of a New Torque and Flux Controllers for Direct Torque Control (DTC) of Induction Machine Utilizing Digital Signal Processor (DSP) and Field Programmable Gate Arrays (FPGA)

CL Toh, NRN Idris*, AHM Yatim, ND Muhamad
Department of Energy Conversion
Universiti Teknologi Malaysia
51310 UTM, Johor, MALAYSIA
*Email: nikrumzi@ieee.org

M. Elbuluk,
Department of Electrical Engineering
University of Akron, Ohio, USA
Email: melbuluk@uakron.edu

Abstract— **This paper presents the simulation and experimental results of a new torque and flux controllers for the direct torque control (DTC) of induction motor drives. The controllers provide a simple solution to the variable switching frequency and high torque ripples problems encountered in the hysteresis-based DTC drives. The controllers operate based on the comparison between the compensated error signals and the triangular waveforms. Implementation of these controllers using the combination of a digital signal processor (DSP) and a field programmable gate array (FPGA) device is presented. The simulation and experimental results showed that the controllers were capable of reducing the torque and flux ripples significantly. At the same time the switching frequency was fixed, independent of the operating conditions.**

.

I. INTRODUCTION

Direct torque control of induction motor has gained popularity in industrial applications mainly due to its simple control structure. Since it was first introduced in 1986 [1], several modifications and improvements have been made to the original control structure in order to overcome two major problems normally associated with DTC, namely the high electromagnetic torque ripple and variable switching frequency. It is well established that these problems are mainly due to the use of hysteresis torque and flux controllers. For this reason, most of the methods used to overcome these problems were accomplished by replacing the hysteresis- with the non-hysteresis -based controllers.

Without the hysteresis controllers, there are two different types of approaches normally used. The first approach is to generate a reference stator voltage vectors that will force the torque and flux to follow their reference values. Using this approach, the voltage vector selection table is removed and the desired stator voltage is normally implemented using space vector modulation. There are several variations used to obtain the reference voltage vectors, which were discussed in [2]. The second type of approach is to retain the voltage vector selection table but the torque controller switching is performed at regular intervals with zero voltage vectors introduced between the sampling. By introducing zero voltage vectors, the torque ripple and the switching frequency are reduced and increased, respectively. The task is therefore to calculate appropriate duration of the zero voltage vectors to produce the desired average torque, which equals the reference torque. Several methods had been

proposed, such as by using complex mathematical equations or fuzzy controllers [3-5]. Both approaches have, to some extent, managed to reduce torque ripple and maintained a constant switching frequency. However, they have, at the same time, significantly increased the complexity of the DTC drive. This is obviously a major disadvantage as far as the implementation is concerned since it will require faster processor, particularly when small torque ripple is desired.

In our previous paper [6] we have introduced a new torque and flux controllers to replace the conventional hysteresis controllers. The effectiveness of the controllers was analyzed through simulations. This paper presents the hardware implementation of our proposed controllers. Due to the principle of the controllers, which is based on waveform comparisons, the implementation is relatively easy. In this paper, the FPGA device was used to perform the waveform comparisons and the DSP was used to estimate the torque and stator flux. The paper is organized as follows. The second section presents the principle and modeling of our proposed controllers. Section 3 discusses on the design and implementation of the controllers. In section 4 we present some simulation and experimental results. Finally, conclusion is given in section 5.

II. PRINCIPLE AND MODELING OF THE PROPOSED CONTROLLERS

The simple structure of the DTC drive will not be affected with the application of the proposed controllers. The hysteresis comparators, are removed and replaced with the constant frequency controllers, as depicted in Fig. 1. This section discusses on the working principle of the proposed torque and flux controllers. The small signal models of the torque and flux loops are also presented.

A. Torque controller

The proposed torque controller consists of two triangular waveform generators, two comparators and a PI controller as shown in Fig. 2. The two triangular waveforms (C_{upper} and C_{lower}) are 180° out of phase with each other. The absolute values of the DC offsets for the triangular waveforms are set to half of their peak-peak values. In principle, the output of the proposed torque controller is similar to that of the three-level hysteresis comparator [1], which can be either of three states: −1, 0 or 1. If the output is either 1 or −1, active

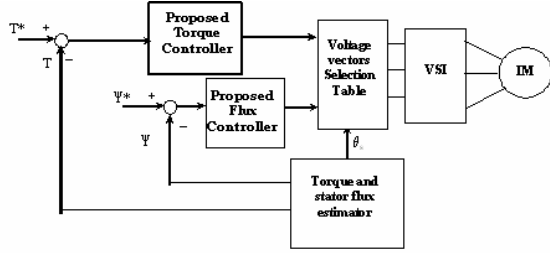voltage vectors are applied and if the output is 0, zero vectors are applied.

Fig. 1 DTC drive with the proposed torque and flux controllers

The value of the instantaneous output of the torque controller designated by $q_t(t)$ is given by (1). For a triangular period of $T_{tri,t}$, its averaged value which is designated by d_t is given by (2).

$$q_t(t) = \begin{cases} 1 & \text{for } T_c \geq C_{upper} \\ 0 & \text{for } C_{lower} < T_c < C_{upper} \\ -1 & \text{for } T_c \leq C_{lower} \end{cases} \quad (1)$$

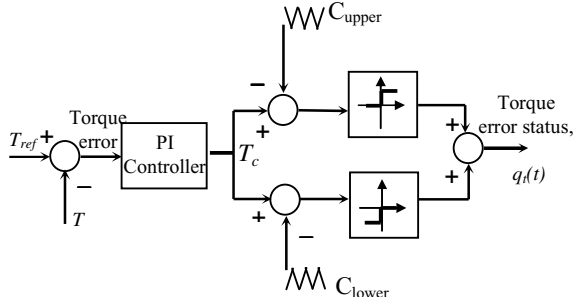$$d_t(t) = \frac{1}{T_{tri,t}} \int_t^{t+T_{tri,t}} q(t)\, dt \quad (2)$$

Fig. 2 Proposed torque controller

In order to properly design the PI controller, a small signal model of the torque loop has to be developed. The space vector equations of induction machine expressed in general rotating frame are given by:

$$\overline{v}_s^g = R_s \overline{i}_s^g + \frac{d\overline{\psi}_s^g}{dt} + j\omega_g \overline{\psi}_s^g \quad (3)$$

$$0 = R_r \overline{i}_r^g + \frac{d\overline{\psi}_r^g}{dt} + j(\omega_g - \omega_r)\overline{\psi}_r^g \quad (4)$$

In the equations (3) and (4), $\overline{\psi}_s^g$ and $\overline{\psi}_r^g$ are the stator and rotor flux linkages respectively and are given by:

$$\overline{\psi}_s^g = L_s \overline{i}_s^g + L_m \overline{i}_r^g \quad (5)$$

$$\overline{\psi}_r^g = L_r \overline{i}_r^g + L_m \overline{i}_s^g \quad (6)$$

The super-script 'g' in the above equations denotes that the quantity is referred to the general reference frame. The torque and mechanical dynamics of the machines are modeled by the following:

$$T_e = \frac{3}{2}\frac{p}{2}\overline{\psi}_s^g \times \overline{i}_s^g \quad (7)$$

$$J\frac{d\omega_m}{dt} = J\frac{2}{p}\frac{d\omega_r}{dt} = T_e - T_{load} \quad (8)$$

It has been shown in our previous paper [6] that using the space vector equations of the induction machine given in (3)-(6), the positive and negative torque slopes in stator flux reference frame can be written as

$$\frac{dT_e^+}{dt} = -\frac{T_e}{\sigma\tau_{sr}} + \frac{3p}{4}\frac{L_m}{\sigma L_s L_r}\left[v_s^{\psi_s}\psi_s - (\omega_r - \omega_{\psi_s})\cdot(\psi_s\psi_r^{\psi_s})\right] \quad (9)$$

$$\frac{dT_e^-}{dt} = -\frac{T_e}{\sigma\tau_{sr}} - \frac{3p}{4}\frac{L_m}{\sigma L_s L_r}\left[(\omega_r - \omega_{\psi_S})\cdot(\psi_s\psi_r^{\psi_S})\right] \quad (10)$$

The superscript $\omega_{\psi s}$ in (9) and (10) indicates that quantities are referred to the stator flux reference frame and $\frac{1}{\sigma\tau_{sr}} = \left(\frac{1}{\sigma\tau_s} + \frac{1}{\sigma\tau_r}\right)$, where σ, τ_s, τ_r are the total leakage factor, stator time constant and rotor time constant respectively. Since we know that the number of active voltage vectors selected over one synchronous cycle is given by $2\pi f_{tri}/\omega_e$, where ω_e is the synchronous frequency and f_{tri} is the triangular frequency, the ratio between the small change in stator flux angle ($\Delta\theta$) and the duration of active voltage vectors applied (Δt) is given by

$$\frac{\Delta\theta}{\Delta t} = \frac{\left(\frac{2\pi\omega_e}{2\pi f_{tri}}\right)}{\frac{d_t}{f_{tri}}} = \frac{\omega_e}{d_t} \quad (11)$$

Assuming that Δt is small enough such that the change in stator flux is linear, (11) approximates $\omega_{\psi s}$; i.e. $\omega_{\psi s} d = \omega_e$ Therefore the instantaneous stator flux frequency can be written in terms of average duty ratio d_t and rotor speed as

$$\omega_{\psi s} = \frac{\omega_{slip} + \omega_r}{d_t} \quad (12)$$

Substituting (12) into (9) and (10) and averaging these equations [6] gives

$$\frac{dT_e}{dt} = -A_t T_e + B_t v_s^{\psi s} d + K_t\left(\omega_{slip}\right) \quad (13)$$

where $A_t = \frac{1}{\sigma\tau_{sr}}$, $B_t = \frac{3p}{4}\frac{L_m}{\sigma L_s L_r}\psi_s$, $K_t = \frac{3p}{4}\frac{L_m}{\sigma L_s L_r}(\psi_s\psi_r^{\psi_s})$

In (13) it is assumed that the magnitudes of the stator and rotor fluxes are held constant. Equation (13) can now be transformed to frequency domain and linearized by introducing small perturbation in T_e, d_t and ω_{slip}. The torque, T_e therefore can be written as

$$\tilde{T}_e(s) = \frac{B_t v_s^{\psi s} \tilde{d}_t(s) + K_t \tilde{\omega}_{slip}(s)}{s + A_t} \qquad (14)$$

The term contributed by the slip frequency is relatively small and hence for simplicity will be neglected. The small signal torque loop is shown in Fig 3. Ideally, the torque loop bandwidth should be as large as possible to obtain fast torque response. However, the bandwidth and hence the selection of controller's parameters (proportional gain K_{tp}, and integral gain K_{ti}) is limited by either the triangular frequency or the sampling period, depending on which one is lower. This means that we can increase the inverter switching frequency much higher than the sampling frequency provided that the bandwidth is limited by the sampling frequency. Since the triangular waveform is generated using the FPGA device, its frequency can be few times higher than the sampling frequency. It is, however, necessary to synchronize the sampling and the triangular waveforms.
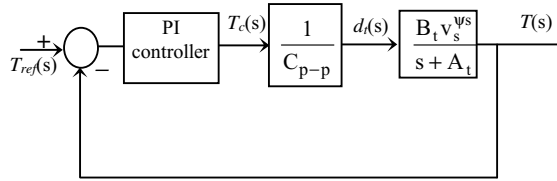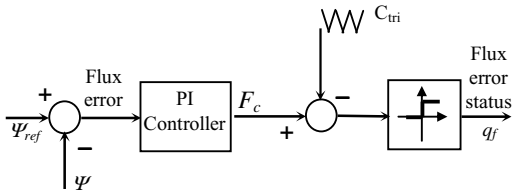

Fig. 3 Small signal torque loop

Fig. 4 Proposed flux controller

B. Flux Controller

The proposed flux controller is shown in Fig 4, which in principle works similar to that of the torque controller. As in the hysteresis-based controller, there are only two levels of output generated from the controller, i.e. 1 to increase the flux and 0 to reduce the flux. This implies that only single triangular waveform is required. For a given synchronous frequency, the switching frequency of the flux controller

only depends on the triangular waveform frequency. The output of the controller is given by

$$q_f(t) = \begin{cases} 1 & \text{for } F_c \geq C_{tri} \\ 0 & \text{for } F_c < C_{tri} \end{cases} \qquad (15)$$

For a triangular period of T_{tri}, its average value is given by

$$d_f(t) = \frac{1}{T_{tri,f}} \int_t^{t+T_{tri,f}} q(t) \, dt \qquad (16)$$

For the sake of simplicity, we will assume that the stator resistance drop is negligible, hence using (3), the slope of the flux in stationary reference frame can be approximated by (17) which simply indicate that it is totally depends on the selected voltage vectors.

$$\text{slope} \equiv \frac{d\overline{\Psi}}{dt} = \overline{v}_s \qquad (17)$$

The derivative of the stator flux vector at t is the tangent vector of the stator flux to the curve traced by $\overline{\psi}_s$ at t. Therefore the slope depends on the stator flux position and it can be seen from Fig. 5 that at every entrance of a sector, the magnitude of the positive and negative slopes are zero and maximum, respectively.
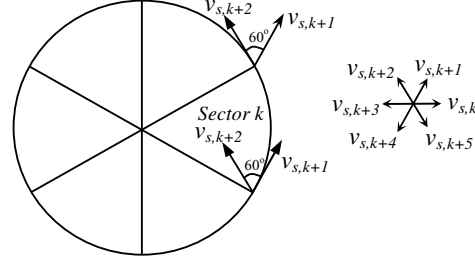

Fig.5 Circular flux locus

If θ is the angle of the stator flux relative to the sector it enters, the positive and negative slopes can be written as

$$\left. \begin{aligned} \text{slope}^+ &\equiv \frac{2}{3} V_{dc} \sin\theta \\ \text{slope}^- &\equiv -\frac{2}{3} V_{dc} \sin(\theta + \frac{2}{3}\pi) \end{aligned} \right\} \qquad (18)$$

For simplicity it will be assumed that the slope is constant during which the flux error status is 1 or 0. Then, it is possible to obtain the average positive and negative slopes by averaging them over a sector. This is easily done since we know the number of positive or negative slopes within a sector is given by $N_f = (2\pi f_{tri})/6\omega_e$. The average positive and negative slope can be calculated as

$$\frac{d\Psi^+}{dt} = \frac{1}{N_f} \sum_{n=0}^{N_f} \frac{2}{3} V_{dc} \sin\left(\frac{\frac{\pi}{3}}{N_f}\right) n = A_\psi \qquad (19)$$

$$\frac{d\Psi^-}{dt} = -\frac{1}{N_f} \sum_{n=0}^{N_f} \frac{2}{3} V_{dc} \sin\left(\left(\frac{\frac{\pi}{3}}{N_f}\right)n + \frac{2}{3}\pi\right) = B_\psi \qquad (20)$$

Which gives an average slope of

$$\frac{d\Psi}{dt} = \left(A_\psi - B_\psi\right)d_f + B_\psi \qquad (21)$$

Introducing small perturbation in ψ and d_f, the transfer function between ψ and d can be obtained as

$$\frac{\tilde{\Psi}}{\tilde{d}_f} = \frac{\left(A_\psi - B_\psi\right)}{s} \qquad (22)$$

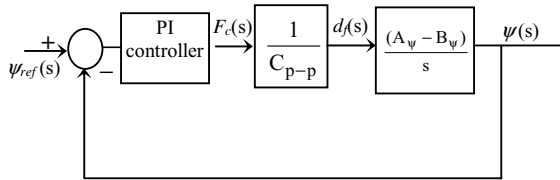Finally, the small signal flux loop is shown as in Fig 6.


Fig. 6 Small signal flux loop

It is clear from the small signal model that only proportional type controller is required to obtain zero steady state error in flux response. Similar to torque control, the bandwidth is limited by the triangular frequency or the sampling frequency, depending on which one is lower. Provided that the sampling is synchronized with the triangular waveform, the switching frequency can be made higher than the bandwidth of the flux loop.

III. IMPLEMENTATION OF THE PROPOSED CONTROLLERS

The major parts of the controllers were composed of a DSP and an FPGA device. With this combination, it is possible to generate the triangular waveforms at frequencies close to or higher than the sampling frequency of the DSP. Therefore as discussed in the previous section, it is possible to increase the switching frequency of the inverter much higher than the sampling period.

The DSP board (DS1102) from dSPACE, based on TMS320C31 operating at 60 MHz, was used in this paper. It was mainly used to estimate the torque and stator flux using the stator current and voltage, which were sampled at 20.8 kHz (DSP sampling period T_{DSP} = 48 s) . Other than this, the DSP was also responsible for 1) implementing the PI and P controllers for the torque and flux loops, respectively and 2) determining the sector of the stator flux. These values were then passed to the Altera EPF10K20 FPGA device contained on an Altera UP1 Educational Board. Very high-speed integrated circuits Hardware Description Language (VHDL) was utilized in digital logic designs of the FPGA. The design was then compiled and simulated using MAX +

PLUS II and finally downloaded to the EPF10K20 device. Since the triangular waveforms of the torque and flux controllers were generated using FPGA, their frequencies were not constrained by the clock speed of the DSP. In this paper, the torque and flux triangular frequencies are set to 10.4 kHz and 5.2 kHz, respectively and they are synchronized with the sampling frequency of the DSP – this is illustrated in Fig. 7. The torque and flux errors which were obtained from the DSP, were compared with the triangular waveforms within the FPGA. From the comparison results and the location of the stator flux, suitable voltage vectors were selected. The various tasks of the DSP and the FPGA were summarized in Fig. 8.
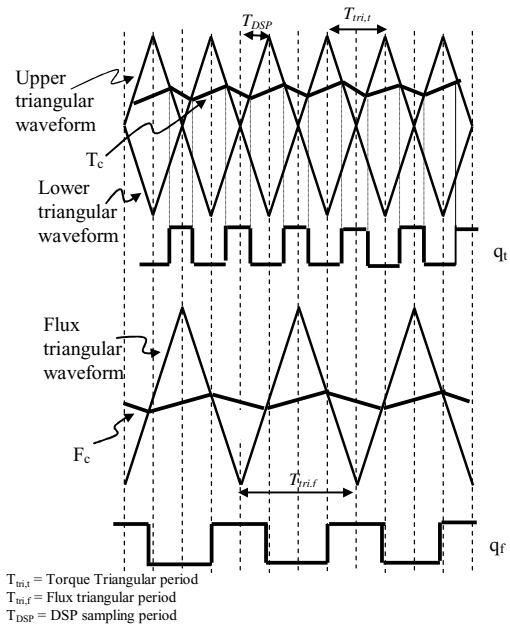
$T_{tri,t}$ = Torque Triangular period
$T_{tri,f}$ = Flux triangular period
T_{DSP} = DSP sampling period

Fig. 7 Ideal timing diagram of the proposed torque and flux controllers

IV. SIMULATIONS AND EXPERIMENTAL RESULTS

Using the design procedure described in Section II, proportional and integral constants for the PI torque controller were calculated as K_p = 180 and K_i = 6000. With these values, the torque loop bandwidth is found out to be 1885 rad/s. For this particular design, the bandwidth is limited by the triangular frequency, since the triangular frequency is lower than the sampling frequency. It should be noted that it is possible to increase the inverter switching frequency higher than the DSP sampling frequency by increasing the triangular frequency. Under this condition, the controller should be designed such that the bandwidth is constrained by the DSP sampling frequency. As for the flux loop bandwidth, it can be adjusted by simply varying the gain of the flux proportional controller. It was found out that the value of K_{pf}=11000 gives flux bandwidth of 15268 rad/s.
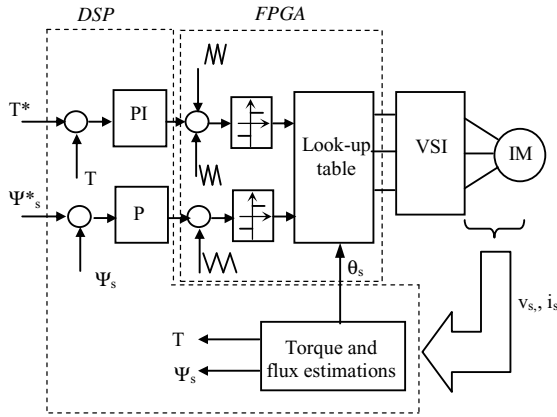
Fig. 8 Implementation of the proposed controllers using DSP and FPGA

Three different sets of simulations and experiments were carried out as follows:

i) Hysteresis torque and flux controllers,
ii) Proposed torque controller and hysteresis flux
iii) Proposed torque and flux controllers

The simulations of the DTC drive were carried out using Matlab/Simulink simulation package. The parameters of the induction machine used in the simulation and experiment are listed in Table 1.

TABLE I
PARAMETERS OF INDUCTION MACHINE AND SETTINGS

Stator resistance	10.9 Ω
Rotor resistance	9.5 Ω
Stator self inductance	0.859 H
Rotor self inductance	0.859 H
Mutual inductance	0.828 H
Rated speed	2880 rpm
Pole pair	2
DC link voltage	120 V
Rated flux	0.495 Wb

Fig. 9 shows the simulation and experimental results of a torque response for a step reference step from -0.6 Nm to 0.6 Nm. Experimental results for the torque and flux hysteresis controllers shows a significant ripple due to the sampling delay in the DSP. This cannot be seen in the simulation since the model does not include the sampling delay. All of the three sets of controllers show an excellent torque response, however the ones with the proposed torque controller produce significant torque ripple reduction. Fig. 10 shows the steady state current and line-line voltage for the three different sets of controllers. The corresponding steady state stator flux locus is shown in Fig. 11. Clearly, with the proposed torque and flux controllers, current distortion and stator flux ripple are significantly reduced.
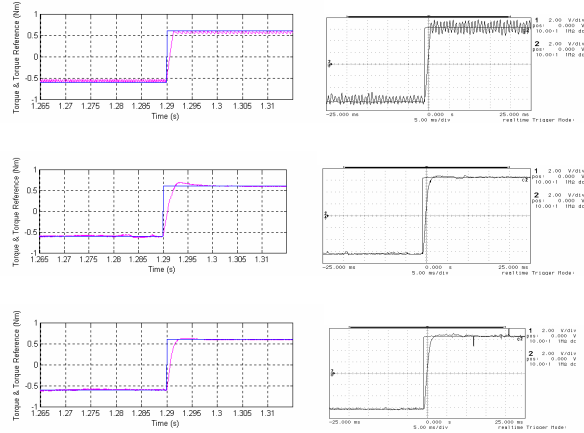

Fig. 9 Step torque response. Experimental results scale of 0,2 Nm/div. (a) hysteresis torque and flux controllers, (b) Proposed torque and hysteresis flux controllers, (c) proposed torque and flux controllers.

In order to investigate the dynamic performance of the proposed controllers, a speed loop was constructed using a low resolution incremental encoder as a speed sensor (200 ppr). A square wave speed reference was applied and the experimental results of the speed and torque responses are shown in Fig. 12. The figure clearly indicates an excellent dynamic performance of the proposed controller with significant torque ripple reduction. Finally, to look at the switching frequency of the inverter, a square wave torque reference of ±0.6 Nm was applied and the frequency spectrum of a switching leg was recorded as in Fig. 13. The hysteresis-based controller produced an unpredictable and dispersed switching harmonics, whereas for the proposed controllers, the harmonic component is concentrated around the carrier frequency and its multiple. The first harmonic appeared at 10.4 kHz, which is equivalent to the torque loop triangular waveform frequency.
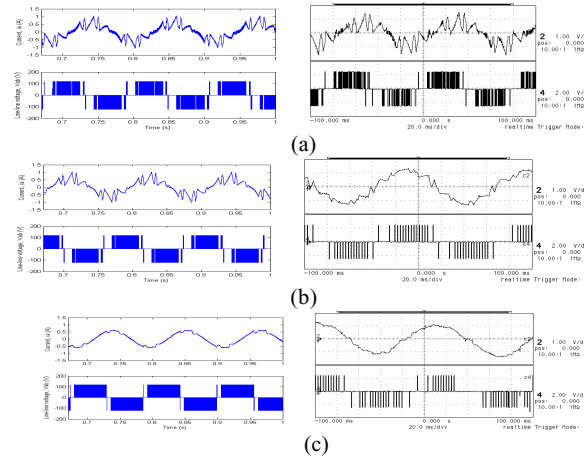

Fig.10 Simulation and experimental (0.5714A/div, 100V/div) results of steady state phase current and line-line voltage. (a) Hysteresis-based torque and flux controllers, (b) Proposed torque and hysteresis-based flux controllers, (c) Proposed torque and flux controllers
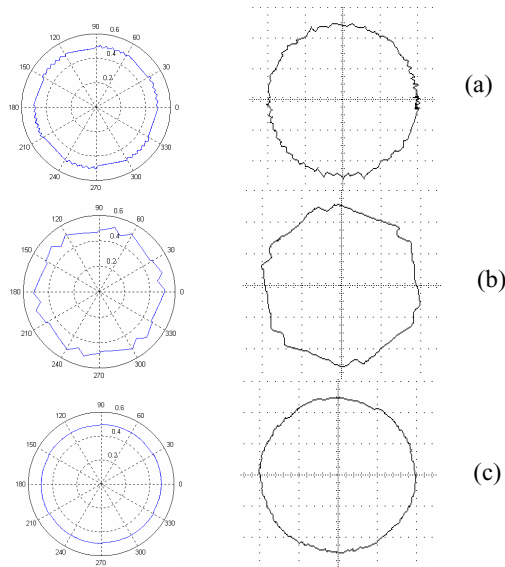
1598

Fig. 11 Simulation and experimental stator flux locus (0.2 Wb/div) for (a) Hysteresis-based torque and flux controllers, (b) Proposed torque and hysteresis-based flux controllers, (c) Proposed torque and flux controllers
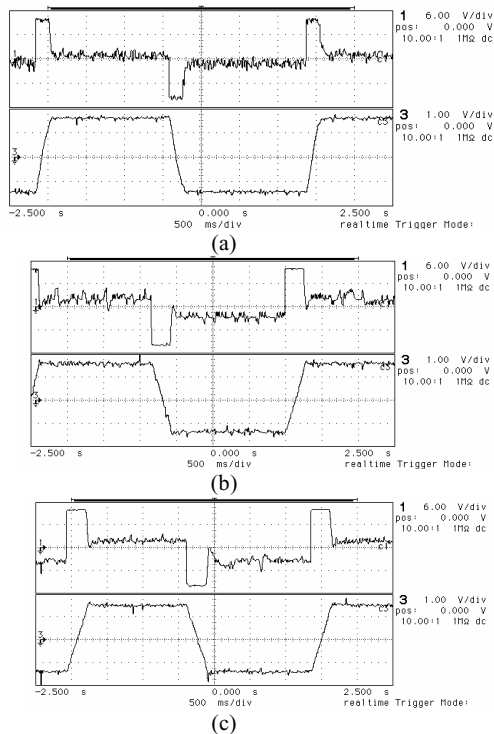

Fig. 12 Experimental results. Torque (1 Nm/div) and speed (9.33 rad/s/div) response with square wave speed reference. (a) Hysteresis torque and flux controllers, (b) Proposed torque and hysteresis-based flux controllers, (c) Proposed torque and flux controllers
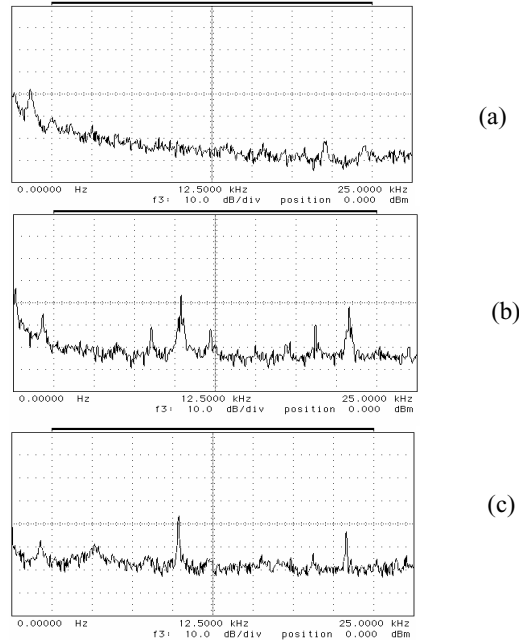

Fig. 13 Frequency spectrum of the switching leg (a) Hysteresis-based torque and flux controllers, (b) Proposed torque and hysteresis-based flux controllers, (c) Proposed torque and flux controllers

V. CONCLUSION

The paper has presented the new torque and flux controllers with constant switching frequencies. Small signal modeling of the torque and flux loops has been presented. The simulation and implementation of the DTC drive with the proposed controllers were presented. From the simulation and experimental results, it is shown that despite of their simple control structure and implementation, the proposed controllers have managed to significantly reduce the torque and flux ripples.

REFERENCES

[1] I. Takahashi and T. Noguchi, A new quick-response and high-efficiency control strategy of an induction motor , *IEEE Trans. Ind. Appl.*, Vol. IA-22, No 5, pp. 820-827, 1986

[2] G. S. Buja,; M. P. Kazmierkowski, Direct torque control of PWM inverter-fed AC motors - a survey , *IEEE Trans. On Industrial Electronics*, vol. 51, No. 4 , pp. 744 – 757, Aug. 2004

[3] S. Mir, and M. E. Elbuluk, Precision torque control in inverter-fed induction machines using fuzzy logic , *IEEE-IAS Annual Meeting*, pp. 396-401, 1995.

[4] I. G. Bird, and H. Zelaya De La Parra, Fuzzy logic torque ripple reduction for DTC based AC drives , *Electronic Letters*, Vol. 33, No.17, pp. 1501-1502, 1997

[5] J. K. Kang and S. K. Sul, Torque ripple minimization strategy for direct torque control of induction motor, in *Conf. Rec. IEEE-IAS Annu. Meeting*, pp. 438-443, 1998

[6] N. R. N. Idris, A. H. M. Yatim, N.D. Muhamad and T. C. Ling, Constant frequency torque and flux controllers for direct torque control of induction machines , *34th Annual IEEE Power Electronics Specialist Conference*, PESC'03, Vol. 3, pp. 1095-1100, 2003